

# DSAGL: Dual-Stream Attention-Guided Learning for Weakly Supervised Whole Slide Image Classification

Daoxi Cao<sup>a</sup>, Hangbei Cheng<sup>a</sup>, Yijin Li<sup>b</sup>, Ruolin Zhou<sup>a</sup>, Xuehan Zhang<sup>a</sup>, Xinyi Li<sup>c</sup>, Binwei Li<sup>a</sup>, Xuancheng Gu<sup>d</sup>, Jianan Zhang<sup>e</sup>, Xueyu Liu<sup>c,\*</sup> and Yongfei Wu<sup>c,\*</sup>

<sup>a</sup>College of Computer Science and Technology (College of Data Science), Taiyuan University of Technology, Taiyuan, Shanxi, 030024, China

<sup>b</sup>College of Humanities, Law and Foreign Languages, Taiyuan University of Technology, Taiyuan, Shanxi, 030024, China

<sup>c</sup>College of Artificial Intelligence, Taiyuan University of Technology, Taiyuan, Shanxi, 030024, China

<sup>d</sup>School of Cyberspace Security, Beijing University of Posts and Telecommunications, Beijing, 102206, China

<sup>e</sup>School of mathematics, Taiyuan University of Technology, Taiyuan, Shanxi, 030024, China

## ARTICLE INFO

**Keywords:**

Pathology Image Classification

Multiple Instance Learning

Teacher-Student Network

Attention Mechanism

## ABSTRACT

Whole Slide Images are critical for cancer diagnosis due to their ultra-high resolution and rich semantic content. However, their massive size and the limited availability of fine-grained annotations pose substantial challenges for conventional supervised learning. We propose the dual-stream attention-guided learning framework called DSAGL, a novel weakly supervised classification framework that combines a teacher-student architecture with a dual-stream design. DSAGL explicitly addresses instance-level ambiguity and bag-level semantic consistency by generating multi-scale attention-based pseudo labels and guiding instance-level learning. A shared lightweight encoder enables efficient long-range dependency modeling, while a fusion-attentive module enhances focus on sparse but diagnostically relevant regions. We further introduce a hybrid loss to enforce mutual consistency between the two streams. Experiments on CIFAR-10, NCT-CRC, and TCGA-Lung datasets demonstrate that DSAGL consistently outperforms state-of-the-art MIL baselines, achieving superior discriminative performance and robustness under weak supervision.

## 1. Introduction

In the field of digital medicine, ultra-high-resolution Whole Slide Images (WSIs) have become a core imaging modality in modern pathological diagnosis due to their comprehensive and information-rich representation [35, 42, 8, 49]. WSIs can capture microscopic tissue structures with exceptional precision, providing critical support for cancer diagnosis and treatment planning. However, their massive size imposes substantial computational burdens [11, 43]. The complexity of tissue structures further complicates the accurate identification of abnormal regions, which often exhibit diffuse and scattered morphological features that hinder automated analysis. Traditional supervised learning methods rely heavily on exhaustive annotations by expert pathologists—a process that is not only time-consuming and costly but also subject to significant inter-observer variability, ultimately compromising model generalization. To address these challenges, weakly supervised learning approaches have gained increasing attention in computational pathology [27, 29, 34, 38, 44]. By leveraging easily accessible patient-level labels, these methods reduce the dependency on high-quality annotations and offer a promising pathway toward efficient and accurate analysis of large-scale pathological images.

In recent years, significant progress has been made in WSI classification for computational pathology, achieving notable progress. Among these approaches, multiple instance learning (MIL) [18, 19, 26, 31] has emerged as a dominant paradigm. MIL-based methods typically regard a WSI as a "bag" composed of numerous image patches and leverage patient-level labels to guide instance-level learning [50, 3]. This formulation not only makes effective

\*Xueyu Liu and Yongfei Wu are Corresponding authors

✉ caodaoxi6432@link.tyut.edu.cn (D. Cao); chenghangbei0702@163.com (H. Cheng); liyijin4335@link.tyut.edu.cn (Y. Li); zhouruolin4817@link.tyut.edu.cn (R. Zhou); zhangxuehan7154@link.tyut.edu.cn (X. Zhang);

lixinyi7064@link.tyut.edu.cn (X. Li); libinwei7791@link.tyut.edu.cn (B. Li); guxuancheng@bupt.edu.cn (X. Gu);

zhangjiananm0@sina.com (J. Zhang); liuxueyu0229@link.tyut.edu.cn (X. Liu); wuyongfei@tyut.edu.cn (Y. Wu)

ORCID(s): 0009-0003-7157-4802 (D. Cao); 0009-0006-7310-7636 (H. Cheng); 0009-0008-3418-0253 (Y. Li); 0009-0007-6038-7170 (R. Zhou); 0009-0001-3734-8874 (X. Zhang); 0009-0006-3743-8411 (X. Li); 0009-0007-7263-7720 (B. Li); 0009-0009-8980-434X (X. Gu); 0009-0001-0147-0990 (J. Zhang); 0000-0001-5745-4722 (X. Liu); 0000-0002-5010-2561 (Y. Wu)

use of coarse-grained annotations but also aligns well with clinical diagnostic practices, significantly reducing the cost of data labeling while delivering promising results across various tasks. However, existing MIL methods often rely on the assumption that instances within a bag are independent and identically distributed (i.i.d.), or adopt simplistic aggregation strategies such as attention-based pooling [19]. These approaches are limited in their ability to capture complex spatial dependencies and contextual information that are critical for accurately identifying diagnostic regions. The lack of long-range modeling across spatially distant patches hinders precise localization and recognition of relevant lesions, especially in real-world scenarios characterized by sparse and heterogeneous pathological patterns. Moreover, a fundamental trade-off persists between instance-level discriminability and bag-level classification performance, which compromises the model's generalization and clinical applicability. Therefore, under weak supervision, designing more expressive and context-aware architectures that can jointly enhance instance-level and bag-level performance remains a central challenge in computational pathology.

Despite significant progress in improving diagnostic accuracy and computational efficiency for WSI classification, current methods still face two fundamental challenges that severely limit their robustness and generalization capabilities. First, most existing approaches rely on convolutional neural networks (CNNs) [1] or Transformer-based architectures [14, 30]. CNNs are constrained by their limited receptive fields, making it difficult to effectively model long-range dependencies [12, 17, 52]. Transformers, while capable of capturing global context, suffer from quadratic computational complexity with respect to the number of instances, resulting in poor scalability and inefficiency in high-resolution WSI scenarios [52, 17]. Second, conventional attention mechanisms tend to focus on densely textured or visually consistent regions, often overlooking sparse yet diagnostically critical instances. This issue is particularly pronounced in widely used single-stream MIL architectures [20], which lack explicit mechanisms for semantic refinement and instance-level disambiguation. As a result, such models often struggle to accurately discriminate key features at the instance level, leading to reduced robustness and generalization in the presence of complex and heterogeneous lesions (see Fig. 1(a)). To address these limitations, the emergence of Mamba offers a promising new approach for modeling long-range dependencies. By enabling efficient global context modeling with linear computational complexity, Mamba significantly reduces the processing cost of large-scale instance sets without compromising performance.

To address the aforementioned challenges, we propose DSAGL (Dual-Stream Attention-Guided Learning), a novel weakly supervised classification framework based on a dual-stream, teacher-student architecture with attention guidance. DSAGL is designed to capture inter-instance correlations while jointly enhancing both instance-level discriminability and bag-level classification performance in MIL models. The framework consists of a unified feature extraction backbone and a dual-stream structure. Specifically, the teacher stream employs a multi-scale attention mechanism to focus on diagnostically relevant instances, enabling accurate bag-level classification while generating high-quality soft pseudo labels. Guided by these pseudo labels, the student stream performs instance-level classification, thereby improving fine-grained discriminative capability. Moreover, as shown in Fig. 1(b), DSAGL employs an alternating training strategy between the teacher and student networks, in contrast to the sequential paradigm adopted by conventional dual-stream models. This collaborative optimization enhances semantic consistency and further improves the overall model performance.

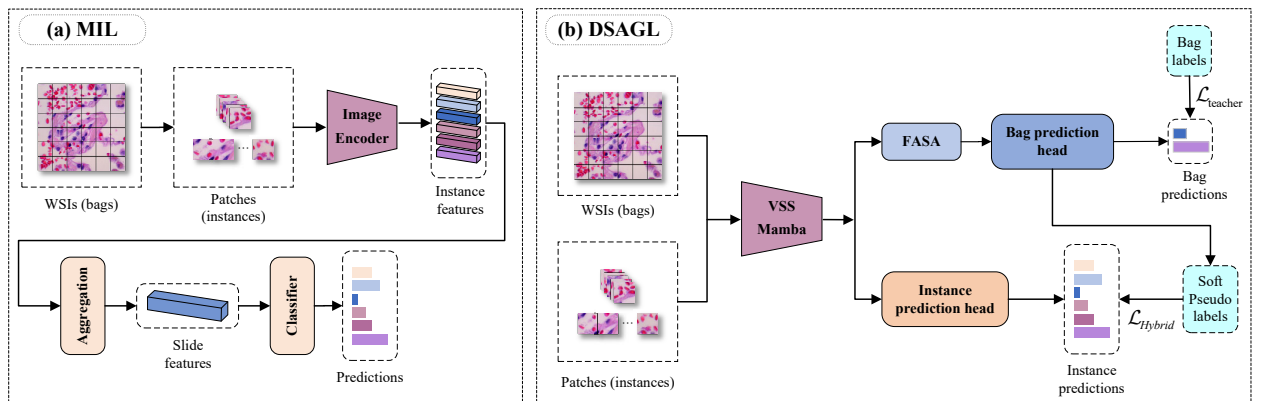


Fig. 1: (a) Basic MIL architecture; (b) Our proposed DSAGL architecture.

To further enhance the model’s representational capacity and generalization under weak supervision, DSAGL incorporates two key components: a Vision-aware Skip-connected Selective Mamba encoder (VSSMamba) for efficient long-range dependency modeling with linear complexity, and a Fusion-Attentive Scale-Aware module (FASA) to emphasize sparse but diagnostically relevant regions. These designs enable DSAGL to effectively leverage coarse-grained labels for accurate WSI classification. Extensive experiments conducted on both two synthetic datasets (CIFAR-10 and NCT-CRC) and one real-world pathological dataset (TCGA-Lung) demonstrate that DSAGL outperforms representative MIL-based approaches at both instance and bag levels, highlighting its strong discriminative power and generalization across diverse scenarios.

The main contributions of this work are summarized as follows:

- We propose a novel weakly supervised classification framework, DSAGL, which integrates a dual-stream architecture with a teacher-student mechanism to jointly optimize instance-level discriminability and bag-level classification performance, addressing the limitations of conventional MIL methods in semantic modeling.
- We introduce an alternating training strategy to enhance semantic consistency, enabling collaborative optimization between the teacher and student branches, which significantly improves the model’s robustness and generalization in complex lesion recognition scenarios.
- A lightweight backbone VSSMamba for efficient long-range dependency modeling and a multi-scale attention module FASA for capturing discriminative patterns in sparse tumor regions.

The remainder of this paper is organized as follows: Section 2 reviews related work and highlights current limitations and challenges. Section 3 focuses on the proposed model architecture, detailing its design and key technical components. Section 4 presents experimental results on three datasets along with ablation studies. Section 5 discusses the strengths and limitations of the proposed approach. Finally, Section 6 concludes the paper and outlines potential directions for future research.

## 2. Related Work

### 2.1. Multiple Instance Learning for WSI Classification

Multiple instance learning (MIL) [47, 40, 40] has become a widely adopted weakly supervised paradigm in computational pathology, particularly well-suited for WSIs, which are characterized by extremely high resolution and large-scale tissue content. In MIL, each WSI is divided into a set of patches (instances) grouped into a bag, with supervision provided only at the bag level. This eliminates the need for dense annotations and significantly reduces manual labeling costs.

Early MIL methods, such as MI-Net [48], employed MIL max or mean pooling to aggregate instance features for bag-level prediction. While computationally efficient, these approaches are limited in their ability to distinguish semantically relevant instances. To address this, Ilse et al. [19] introduced Attention-MIL, which incorporates learnable attention weights to assign importance scores to instances. The framework was further extended to ABMIL by incorporating gated attention mechanisms, thereby improving both aggregation flexibility and interpretability. [19] Subsequent works have explored more expressive instance-level modeling strategies. Chen et al. [5] proposed MSA-MIL by integrating multi-scale feature extraction modules, enhancing sensitivity to fine-grained structural variations. Li et al. [28] introduced SA-MIL, which embeds self-attention into the aggregation process to capture contextual dependencies among instances. DTFD-MIL [50] employs a dual-path differential feature design to strengthen the model’s ability to detect heterogeneous lesion patterns. In addition, DSMIL [26] introduces an explicit instance selection module within a dual-branch structure, enabling collaborative instance- and bag-level decision-making. CLAM [31] incorporates attention pruning to localize diagnostically relevant regions and improve interpretability. Transformer-based frameworks such as TransMIL [39] further extend MIL by modeling global dependencies across instances, exhibiting superior long-range reasoning compared to traditional attention-based models.

Despite these advances, two key limitations remain in current MIL-based approaches. First, most models rely solely on bag-level supervision and lack explicit instance-level guidance, which hinders precise localization of critical pathological regions. Second, attention mechanisms are typically used only for feature aggregation and are not explicitly aligned with classification objectives, limiting their effectiveness under weak supervision.

## 2.2. Dual-Stream Architectures and Knowledge Distillation

Prior to the emergence of dual-stream architectures, extensive research explored the integration of knowledge distillation (KD) into single-branch or loosely coupled frameworks to enhance the representational capacity and training stability of student models. For example, Co-MIL [20] employs a multi-teacher collaborative distillation strategy, where separate teacher models extract global and local semantic information to guide the student through cross-model supervision. GLMC [10] introduces bidirectional guidance between global and local branches, thereby improving the model's ability to capture multi-scale lesion features. Self-Distillation utilizes the historical states of the student model as an implicit teacher, enabling knowledge transfer without additional parameter overhead—an approach particularly suitable for resource-constrained settings. ReNA-KD [51] incorporates region-structured attention maps into the distillation process, enhancing spatial awareness and improving recognition of heterogeneous lesion patterns.

Building upon these foundational works, recent studies have further integrated knowledge distillation into dual-stream frameworks to enhance semantic consistency and cross-branch collaboration. R<sup>2</sup>T-MIL [45] introduces a region-aware token distillation module within a Transformer-based architecture, leveraging spatial attention to guide the student in focusing on diagnostically relevant areas. GLMKD [6] designs a dual-teacher framework with global and local branches, and incorporates a shape transfer loss to reconcile inconsistencies between pseudo labels from different teachers, enabling more accurate boundary modeling and improved training stability under weak supervision.

While recent methods have introduced improvements, many distillation strategies remain constrained by static soft labels and rigid optimization phases. The absence of adaptive feedback mechanisms hampers their capacity to cope with semantic drift and evolving inter-branch representations during training.

## 2.3. Long-Range Dependency Modeling in WSI

WSIs are composed of thousands of image patches and exhibit strong non-local structural characteristics. In pathological diagnosis, spatially distant regions often present semantic dependencies—for example, between tumor boundaries and cores, or between inflamed tissues and surrounding microenvironments. Modeling such long-range dependencies is critical for improving classification accuracy.

Convolutional neural networks (CNNs) [2, 7] are inherently limited by their local receptive fields and struggle to capture global contextual information. To address this, Transformer-based [46, 15] architectures have been introduced. TransMIL [39] is one of the earliest attempts to model inter-patch relationships via self-attention for global bag representation. Vision Transformer (ViT) [9] extends standard Transformer designs to image modeling and has been widely adopted in MIL settings. DTFD-MIL further incorporates feature differencing to enhance the modeling of local-global disparities.

Despite their expressive capacity, Transformer models suffer from high computational cost. The attention mechanism scales quadratically with input size, making it inefficient for WSIs with thousands of patches. This leads to memory bottlenecks and latency issues, hindering real-world deployment. To address these limitations, Structured State Space Models (SSMs) [13] have been proposed as efficient alternatives. S4, introduced by Gu et al., first incorporated continuous-time state-space equations into deep networks for efficient long-range sequence modeling. Building on this, Mamba introduced selective state updates and input gating mechanisms, enabling fine-grained control over information flow while preserving the efficiency of SSMs. Mamba [12, 17, 32] achieves superior parallelism and scalability, outperforming standard Transformers in tasks such as image classification and semantic segmentation.

Derived from the Mamba framework, several variants have been developed. Vision Mamba [52] integrates convolutional pre-processing and spatial shift mechanisms to enhance spatial awareness. T-Mamba [17] introduces temporal decoupling for efficient modeling of non-uniform sequential data. U-Mamba [32] extends the architecture for biomedical image segmentation by incorporating a U-shaped encoder-decoder design with Mamba blocks, enabling long-range context modeling while preserving spatial resolution.

## 3. Method

This section provides a detailed exposition of the proposed methodological framework, encompassing the formal definition of the problem, the overall architectural design of the model, and the construction principles of key components, including the VSSMamba and the Dual-Stream Network.

### 3.1. Task Definition

#### 3.1.1. Multiple Instance Learning (MIL)

We consider weakly supervised pathological image classification under the Multiple Instance Learning (MIL) framework. As illustrated in Fig. 2, unlike traditional supervised learning where each instance is individually labeled, MIL assigns labels only at the bag level, with each bag containing multiple unlabeled instances.

Each WSI is divided into a bag of image patches, where each patch is treated as an instance [19, 27, 29, 41]. A bag is defined as  $B_i = \{x_{i,1}, \dots, x_{i,N_i}\}$ , where  $x_{i,j} \in \mathbb{R}^d$  denotes the  $d$ -dimensional feature vector of the  $j$ -th instance in bag  $i$ , and  $N_i$  is the number of instances.

The dataset is represented as  $D = \{(B_i, y_i)\}_{i=1}^M$ , where only bag-level labels  $y_i \in \{0, 1\}$  are available during training. According to the standard MIL assumption, a bag is positive if it contains at least one positive instance:

$$y_i = \max_{1 \leq j \leq N_i} z_{i,j}, \quad (1)$$

where  $z_{i,j} \in \{0, 1\}$  denotes the (latent) instance label. The goal is to jointly optimize bag-level classification and instance-level discrimination under weak supervision.

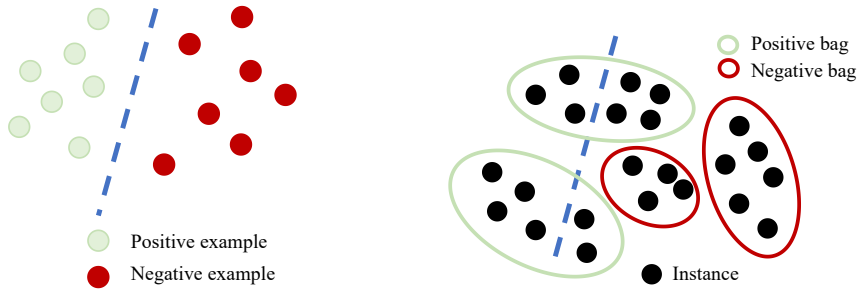


Fig. 2: Supervised learning and Multiple-Instance Learning (MIL).

#### 3.1.2. SSM and Mamba

Structured State Space Models (SSMs) [52] offer an efficient module for long-range sequence modeling with linear time complexity. Given a 1D input sequence  $x(t)$ , the system evolves through a hidden state  $h(t) \in \mathbb{R}^N$ , where  $N$  denotes the dimension of the hidden state, governed by the continuous-time dynamics:

$$\frac{d}{dt}h(t) = \mathbf{A}h(t) + \mathbf{B}x(t), \quad y(t) = \mathbf{C}h(t), \quad (2)$$

where  $\mathbf{A} \in \mathbb{R}^{N \times N}$ ,  $\mathbf{B} \in \mathbb{R}^{N \times 1}$ ,  $\mathbf{C} \in \mathbb{R}^{1 \times N}$  are learnable matrices. For discrete-time processing, we apply zero-order hold (ZOH) with time step  $\Delta$ , yielding:

$$\bar{\mathbf{A}} = \exp(\Delta\mathbf{A}) \quad (3)$$

$$\bar{\mathbf{B}} = (\Delta\mathbf{A})^{-1} (\exp(\Delta\mathbf{A}) - \mathbf{I}) \Delta\mathbf{B} \quad (4)$$

$$h_t = \bar{\mathbf{A}}h_{t-1} + \bar{\mathbf{B}}x_t, \quad y_t = \mathbf{C}h_t \quad (5)$$

The output sequence can also be expressed as a global convolution over a structured kernel:

$$\bar{\mathbf{K}} = \left( \bar{\mathbf{C}}\bar{\mathbf{A}}^i\bar{\mathbf{B}} \right)_{i=0}^{L-1} \quad (6)$$

$$y = \bar{\mathbf{K}} \otimes x \quad (7)$$

where  $\otimes$  denotes one-dimensional convolution. Mamba [12] implements this computation efficiently using either convolution or recurrence, and further enhances it with input-dependent parameterization, enabling scalable modeling for long sequences in applications such as language and video understanding.

### 3.2. Overall Framework

#### 3.2.1. DSAGL architecture

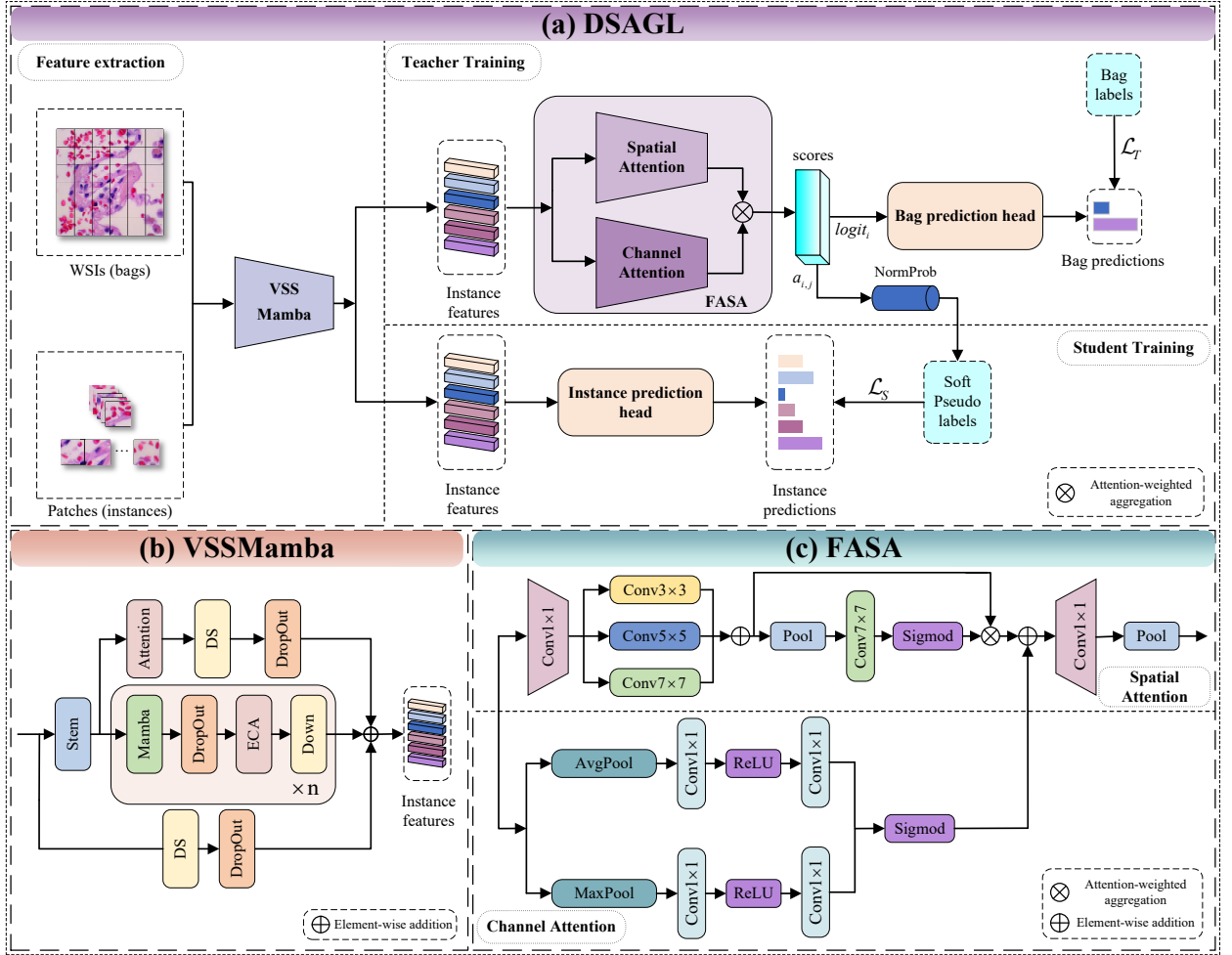


**Fig. 3:** (a) The overall architecture of the proposed Dual-Stream Attention-Guided Learning Weakly Supervised Framework (DSAGL); (b) The proposed Vision-aware Skip-connected Selective Mamba encoder (VSSMamba); (c) The proposed Fusion-Attentive Scale-Aware module (FASA).

To enable efficient and interpretable pathological image classification, we propose a Dual-Stream Attention-Guided Learning framework (DSAGL) for weakly supervised learning. As illustrated in Fig. 3, the DSAGL architecture comprises two main components: a feature extraction module and a dual-stream network consisting of a teacher branch and a student branch. Specifically, we first adopt the Vision-aware Skip-connected Selective Mamba encoder (VSSMamba) to extract initial instance-level features from the input patches. These features are then independently processed by the teacher and student branches. In the teacher branch, we introduce the Fusion-Attentive Scale-Aware (FASA) module to generate bag-level predictions and compute attention scores, which are subsequently used to construct high-quality instance-level pseudo labels. The student branch focuses on fine-grained instance-level classification, guided by the pseudo labels provided by the teacher. Through an alternating training strategy between the two branches, DSAGL enables efficient collaborative feature learning and semantic alignment under weak supervision.

#### 3.2.2. Alternating Training Strategy

To enhance collaborative optimization between the teacher and student networks under weak supervision, DSAGL adopts an alternating training strategy. Instead of relying on conventional joint or sequential training paradigms, this approach updates the two branches in an interleaved manner, enabling iterative refinement of both pseudo labels

and feature representations throughout the training process. During training, the teacher network is updated at fixed intervals, while the student network is continuously optimized using the pseudo labels generated by the teacher. This staged update pattern mitigates potential gradient interference between the two branches and contributes to more stable convergence. By decoupling the training dynamics, each network is able to specialize in its respective task: global bag-level prediction for the teacher and fine-grained instance-level discrimination for the student.

This alternating strategy offers several key advantages. First, it facilitates dynamic refinement of pseudo labels, which are progressively improved during training, thereby reducing the impact of early-stage noise. Second, it enables clear task decoupling, allowing the teacher to focus on holistic feature aggregation while the student learns detailed discriminative representations. Third, the staggered updates improve overall training stability by preventing simultaneous gradient conflicts. Finally, this design proves particularly effective in weakly supervised scenarios, where sparse or noisy labels can severely compromise learning performance.

### 3.3. VSSMamba (Feature Extraction)

Although CNNs [25] and Transformers [46] have excelled in vision tasks, they remain limited in modeling long-range dependencies and incur high computational costs on large-scale WSIs. To address these limitations, inspired by Vision Mamba [52], we propose VSSMamba, a new encoder that extracts discriminative instance-level features with linear complexity.

As illustrated in part (b) of Fig. 3, the VSSMamba comprises a main processing stream and two auxiliary skip connections, enabling enhanced multi-scale and multi-level context fusion. Given an input instance image  $p \in \mathbb{R}^{B \times C \times H \times W}$ , where  $B$ ,  $C$ ,  $H$ , and  $W$  denote the batch size, number of channels, height, and width respectively, we first extract initial features via a convolutional stem layer:

$$f_0 = \text{Stem}(p) \quad (8)$$

The features are subsequently processed by a stack of  $n$  Mamba layers, denoted as  $\{\mathcal{M}_i\}_{i=1}^n$ , along the main path. Each layer consists of a Mamba transformation, followed by Dropout, Efficient Channel Attention  $\mathcal{E}_i$ , and a downsampling operation  $\mathcal{D}_i$ . The number of stacked layers  $n$  can be flexibly adjusted based on data scale and task complexity to balance representation depth and capacity. We denote the final output of the main path as  $f_n$  and output  $f_{i+1}$  of the  $i$ -th layer is computed as:

$$f_{i+1} = \mathcal{D}_i(\mathcal{E}_i(\text{Drop}_i(\mathcal{M}_i(f_i)))) , \quad i = 0, 1, \dots, n-1 \quad (9)$$

To enhance both local detail and global semantics, VSSMamba incorporates two skip connections,  $f_{skip1}$  and  $f_{skip2}$ . The first skip path starts from the stem output  $f_0$ , and passes through a combined attention module consisting of Squeeze-and-Excitation and Spatial Attention  $\mathcal{A}$ . The output is then downsampled and regularized via Dropout to yield locally enhanced features. The second skip path directly downscales the raw input  $p$  to extract global semantic cues:

$$f_{skip1} = \text{Drop}(\mathcal{D}(\mathcal{A}(f_0))) \quad (10)$$

$$f_{skip2} = \text{Drop}(\mathcal{D}(p)) \quad (11)$$

Finally, VSSMamba integrates the outputs from all three paths— $f_n$ ,  $f_{skip1}$ , and  $f_{skip2}$  through a residual aggregation strategy, effectively blending deep semantic features, localized attention-enhanced cues, and global contextual signals. This fusion yields the final instance-level representation  $x$ , which captures both fine-grained structural detail and long-range contextual dependencies crucial for accurate instance discrimination in WSI:

$$x = f_n + f_{skip1} + f_{skip2} \quad (12)$$

In summary, VSSMamba efficiently captures both global dependencies and local details through its hierarchical design with linear-time complexity. By combining the long-range modeling ability of Mamba layers with complementary skip-enhanced feature streams, it provides robust and expressive instance-level representations. This encoder serves as the backbone of our dual-stream framework, enabling effective learning under weak supervision for complex WSI classification tasks.

### 3.4. Duel-Stream Network

To jointly model instance-level and bag-level semantics under weak supervision, we propose a dual-stream architecture comprising a teacher and a student network. This design is motivated by the inherent ambiguity in instance labels within WSIs, where relying solely on bag-level supervision often leads to suboptimal instance discrimination. By decoupling the representation learning into two cooperative branches, the teacher can provide global guidance, while the student focuses on fine-grained instance-level feature extraction.

In this section, we first present FASA, the key attention module designed to enhance the model's ability to extract discriminative features from sparse and ambiguous regions. FASA integrates multi-scale convolution and dual attention mechanisms to address the challenge of lesion heterogeneity and low signal-to-noise ratio. We then elaborate on the functional roles and collaborative interaction between the teacher and student branches, followed by a detailed formulation of the hybrid loss function. This loss is tailored to mitigate the noise and uncertainty introduced by pseudo labels, thus promoting stable optimization and semantic alignment between the two streams.

#### 3.4.1. FASA

To address the challenge of limited supervision, we introduce FASA, a fusion-attentive scale-aware module that enhances feature discriminability by integrating multi-scale convolutional fusion with both channel and spatial attention mechanisms. It performs attention-weighted global pooling to aggregate instance-level features, thereby facilitating discriminative learning in a weakly supervised setting.

As illustrated in part (c) of Fig. 3, FASA improves the discriminability of deep features by integrating spatial and channel attention into a multi-scale fusion framework. Given an input feature map  $x \in \mathbb{R}^{B \times C \times H \times W}$  extracted by the VSSMamba encoder, FASA captures local contextual information at multiple receptive fields through parallel convolutions with kernel sizes of  $3 \times 3$ ,  $5 \times 5$ , and  $7 \times 7$ , where  $C_{k \times k}$  denotes a convolution operation of size  $k \times k$ . The resulting multi-scale features are subsequently concatenated and aggregated along the channel dimension, yielding a unified representation  $h_{fused}$  that preserves complementary information across different spatial scales.

Next, channel and spatial attention mechanisms are independently applied to  $h_{fused}$ , producing two complementary attention-enhanced feature maps:  $f_{channel}$  and  $f_{spatial}$ . These are then combined to obtain the final attentive representation  $f_{out}$ , which integrates both modality-specific importance cues. During instance aggregation,  $f_{out}$  is subjected to global pooling to derive instance-wise attention weights  $a_{i,j}$  and the corresponding bag-level prediction score  $logit_i$ . These outputs jointly serve as weak supervision signals for pseudo-label generation and bag-level classification.

The flow of feature computation is formulated as follows:

$$h_{fused} = \sum_{k \in \{3,5,7\}} C_{k \times k}(x), \quad k \in \{3, 5, 7\} \quad (13)$$

$$f_t = h_{fused} \times \mathcal{A}_t(h_{fused}), \quad t \in \{channel, spatial\} \quad (14)$$

$$f_{out} = f_{channel} + f_{spatial} \quad (15)$$

$$a_{i,j}, logit_i = FASA(f_{out}) \quad (16)$$

By unifying multi-scale feature extraction with spatial and channel-wise attention, FASA provides a powerful mechanism for emphasizing diagnostically relevant regions under weak supervision. Its design allows the network to adaptively aggregate informative patterns across varying spatial resolutions, thereby reinforcing instance-level discriminability and improving the quality of attention-driven pseudo labels essential for downstream tasks.

#### 3.4.2. Teacher Network

The teacher network serves as a bag-level classifier that provides both global predictions and instance-wise guidance under weak supervision. This design enables the decoupling of coarse-grained supervision from fine-grained feature learning, allowing the teacher to learn stable bag-level semantics while generating informative cues for the student network.

Upon receiving instance-level feature vectors, the teacher network employs FASA to compute attention scores for each instance and predicts the bag label via a classification head. The attention mechanism allows the teacher to focus

on diagnostically relevant patches and suppress irrelevant or noisy regions, which is particularly important in WSIs where discriminative signals are sparse and spatially scattered.

Specifically, for each instance  $\{p_{i,j}, j = 1, 2, \dots, n_i\}$  in a bag  $B_i$ , the corresponding feature vector  $x_{i,j}$  is passed into FASA to obtain its attention score  $a_{i,j}$  and the aggregated bag-level logit  $logit_i$ . The attention scores  $\{a_{i,j}\}$  are propagated to the student network as soft supervisory signals, while the logit is further processed by the classification head  $P_t$  to generate the predicted bag label  $\hat{y}_i$ . The bag prediction is supervised using the standard binary cross-entropy loss  $\mathcal{L}_{teacher}$ , which is robust and widely adopted for binary weakly labeled classification tasks. The computation proceeds as follows:

$$a_{i,j}, logit_i = \text{FASA} \left( x_{i,j} \mid x_{i,1}, x_{i,2}, \dots, x_{i,n_i} \right) \quad (17)$$

$$\hat{y}_i = P_t(logit_i) \quad (18)$$

$$\mathcal{L}_T = \mathcal{L}_{teacher}(y_i, \hat{y}_i) \quad (19)$$

By decoupling semantic abstraction and region selection, the teacher network delivers reliable bag-level predictions while producing spatially-aware attention signals. These outputs play a pivotal role in guiding the student network, particularly under noisy and weakly annotated scenarios common in WSI tasks.

### 3.4.3. Student Network

The student network is designed to perform fine-grained instance-level classification under weak supervision. It receives instance feature vectors and predicts the class probability for each individual instance. While sharing the same feature extractor as the teacher network, the student maintains its own classification head  $P_s$ , enabling independent optimization of instance-level representations.

To guide the student in identifying diagnostically relevant regions, the attention score  $a_{i,j}$  provided by the teacher is passed through a normalization module, NormProb, which converts it into a probabilistic pseudo label  $\hat{z}_{i,j}$ . This process stabilizes the supervision signal and helps mitigate early-stage noise in the attention distribution. The training of the student network is supervised using a hybrid loss function  $\mathcal{L}_{Hybrid}$ , which combines cross-entropy loss [33] with Kullback-Leibler divergence [24] in a weighted formulation. This design allows the network to benefit from both hard pseudo labels and soft distribution alignment. The resulting student loss is denoted by  $\mathcal{L}_S$ , and is computed as follows:

$$\hat{z}_{i,j} = \text{NormProb}(a_{i,j}) \quad (20)$$

$$p_{\hat{z}_{i,j}} = P_s(x_{i,j}) \quad (21)$$

$$\mathcal{L}_S = \mathcal{L}_{Hybrid}(\hat{z}_{i,j}, p_{\hat{z}_{i,j}}) \quad (22)$$

By leveraging attention-informed pseudo labels and a tailored hybrid loss, the student network effectively refines instance-level predictions under weak supervision. Its design enables focused learning on diagnostically salient regions and complements the teacher branch by reinforcing semantic consistency at a finer granularity.

### 3.4.4. Hybrid Loss Function

Under weak supervision, instance-level labels are unavailable, and pseudo labels generated by the teacher network are inherently noisy. Relying solely on cross-entropy (CE) loss can lead to overfitting and unstable optimization, especially in early training stages. To address this, we propose a hybrid loss function  $\mathcal{L}_{Hybrid}$  that combines weighted hard-label supervision with soft-label regularization, balancing discriminative learning and robustness.

The student network is supervised by two complementary objectives: a weighted cross-entropy loss  $\mathcal{L}_{CE,student}$  that promotes confident classification based on hard pseudo labels, and a Kullback-Leibler (KL) divergence loss  $\mathcal{L}_{KL,student}$  that aligns the student's output distribution with the teacher's soft predictions. This dual supervision enables sharper

decision boundaries while preserving probabilistic consistency. To mitigate instance-level class imbalance, a weight factor  $w_n$  is applied to negative samples in the CE loss.

Formally, the teacher network is optimized with a bag-level cross-entropy loss:

$$\mathcal{L}_{teacher} = - [y_i \log(\hat{y}_i + \epsilon) + (1 - y_i) \log(1 - \hat{y}_i + \epsilon)], \quad (23)$$

where  $y_i$  denotes the ground-truth bag label,  $\hat{y}_i$  is the predicted bag-level probability, and  $\epsilon$  is a small constant for numerical stability.

$$\begin{aligned} \mathcal{L}_{CE,student} = & -\frac{1}{N} \sum_{i,j} \left[ w_n (1 - \hat{z}_{i,j}) \log(p_{i,j,0} + \epsilon) \right. \\ & \left. + (1 - w_n) \hat{z}_{i,j} \log(p_{i,j,1} + \epsilon) \right] \end{aligned} \quad (24)$$

where  $\hat{z}_{i,j} \in \{0, 1\}$  is the hard pseudo label for instance  $(i, j)$ ,  $p_{i,j,c}$  is the student's predicted probability for class  $c \in \{0, 1\}$ , and  $w_n \in [0, 1]$  controls the relative importance of negative instances.

To leverage soft supervision, the KL divergence loss is introduced as:

$$\mathcal{L}_{KL,student} = T^2 \cdot \frac{1}{N} \sum_{i,j} \sum_{c \in \{0,1\}} q_{i,j,c} \log \left( \frac{q_{i,j,c}}{p_{i,j,c}} \right), \quad (25)$$

where  $q_{i,j,c}$  and  $p_{i,j,c}$  are the predicted class probabilities from the student and teacher, respectively. The temperature parameter  $T > 1$  is used to soften the distributions, and the KL loss is scaled by  $T^2$  to match the magnitude of CE gradients.

The overall student loss is expressed as:

$$\mathcal{L}_{Hybrid} = \alpha \mathcal{L}_{CE,student} + (1 - \alpha) \mathcal{L}_{KL,student}, \quad (26)$$

where  $\alpha \in [0, 1]$  controls the trade-off between hard and soft supervision. The hybrid loss effectively stabilizes learning and improves generalization, particularly under noisy pseudo labels and imbalanced patch distributions.

## 4. Experiment and Results

### 4.1. Datasets

To comprehensively evaluate the performance of DSAGL, we employed three datasets of increasing image resolution, encompassing both synthetic and real-world scenarios, as illustrated in Fig. 4.

#### 4.1.1. Cifar-10

Cifar-10 [23] is a standard image classification dataset consisting of 60,000 color images of size  $32 \times 32$  pixels, divided into 10 classes, with 6,000 images per class. Among them, 50,000 images are used for training and 10,000 for testing. The training set is organized into five batches of 10,000 images each, while the test set constitutes a separate batch. In weakly supervised learning tasks, Cifar-10 is commonly utilized to simulate WSIs by randomly assembling images from different classes to construct synthetic datasets. In our setting, we simulate WSIs by randomly combining images from different classes within the dataset.

#### 4.1.2. NCT-CRC

NCT-CRC-HE-100K [21] is a real-world histopathology image dataset comprising 100,000 non-overlapping image patches extracted from 86 H&E-stained human colorectal cancer and normal tissue slides. All images are of size  $224 \times 224$  pixels and sampled at  $20\times$  magnification. Each image is annotated with one of nine histological tissue classes: adipose (ADI), background (BACK), debris (DEB), lymphocytes (LYM), mucus (MUC), smooth muscle (MUS), normal colon mucosa (NORM), cancer-associated stroma (STR), and colorectal adenocarcinoma epithelium (TUM). Based on this dataset, we constructed multiple subsets with varying positive instance ratios by selecting images from different tissue classes.

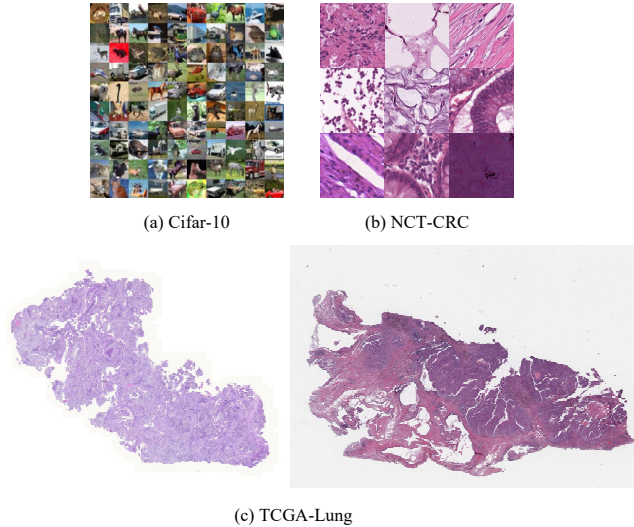


**Fig. 4:** Examples of the three datasets used in our experiments. (a) CIFAR-10, consisting of 10 categories of natural images; (b) NCT-CRC, consisting of 9 categories of colorectal histopathology image patches; (c) TCGA-Lung, consisting of whole-slide images from two lung cancer subtypes.

#### 4.1.3. TCGA-Lung

The TCGA (The Cancer Genome Atlas) lung cancer dataset [26] is an important publicly available resource for histopathological image analysis, encompassing two major subtypes of non-small cell lung cancer: lung adenocarcinoma (LUAD) and lung squamous cell carcinoma (LUSC). The dataset comprises a total of 1,054 high-resolution WSIs stained with hematoxylin and eosin (H&E), provided in the svf format and accessible through the data portal of the National Cancer Institute of the United States. At 20 $\times$  magnification, each WSI is partitioned into approximately 5.2 million image patches of size 224 $\times$ 224 pixels. Each WSI constitutes a bag in the multiple instance learning setting, containing a varying number of tumor and normal patches.

## 4.2. Experimental Details

In the experimental setup, we observe that the instance resolution in the Cifar-10 dataset is relatively low, which makes it less suitable for the Mamba architecture designed for modeling long-range dependencies. Consequently, the number of Mamba layers along the main path (as illustrated in Fig. 3) is set to zero, while the convolutional depth of the Stem module is increased to enhance feature extraction capability. In contrast, for the NCT-CRC and TCGA-Lung datasets, where the instance resolution is higher, the number of Mamba layers is set to 2 and 3, respectively.

In order to facilitate more stable gradient accumulation and efficient parameter updates, we employ the Adam optimizer [22] on NCT-CRC, with a fixed learning rate of 0.0001 and a weight decay of  $e^{-5}$ , and set the batch size to 4. For Cifar-10 and TCGA-Lung, we adopt the SGD optimizer [37] with a learning rate of 0.001 and a batch size of 1. All experiments are conducted on a single NVIDIA V100 GPU.

For both instance-level and bag-level classification tasks, we adopt the area under the ROC curve (AUC) [16] as the primary evaluation metric. Specifically, we report the AUC scores of the DSAGL on both instance-level and bag-level tasks for the synthetic datasets. However, since the TCGA-Lung cancer dataset does not provide ground-truth instance-level labels, we only report the bag-level AUC for this dataset.

## 4.3. Comparison Methods

To systematically evaluate the effectiveness of the proposed DSAGL framework, we compare it against a range of representative multiple instance learning (MIL) approaches. Based on their architectural characteristics, these methods can be categorized into three groups:

**Classical MIL Models.** Representative methods such as MI-Net [48] and RNN-MIL [4] adopt fixed pooling strategies (e.g., max or mean pooling) to aggregate instance features into bag-level representations. While computationally

efficient, these methods lack mechanisms for modeling discriminative regions explicitly and often underperform in weakly supervised scenarios.

**Attention-based MIL Models.** Attention-MIL and its variants, including ABMIL and Gated-ABMIL [19], introduce learnable attention modules to assign instance-specific weights, enabling flexible aggregation and improved interpretability. CLAM [31] further enhances localization by incorporating attention pruning to focus on diagnostically relevant patches.

**Transformer-based or Advanced MIL Models.** This category enhances MIL performance by integrating global context modeling and architectural refinements. TransMIL [39] leverages self-attention to capture inter-instance dependencies; IBMIL [29] introduces region-level interventions for improved instance discrimination; R<sup>2</sup>T-MIL [45] adopts token-level guidance to promote region-aware learning. Our proposed DSAGL also falls into this category, combining dual-stream optimization, attention-guided pseudo supervision, and efficient long-range modeling via the VSSMamba encoder.

All models are evaluated on the CIFAR-10 and NCT-CRC datasets under varying positive instance ratios. Specifically, CIFAR-10 is tested under ratios ranging from 1% to 70%, while NCT-CRC uses ratios from 10% to 70%. For the TCGA-Lung dataset, which lacks instance-level annotations, only bag-level classification performance is reported. Baseline results are either reproduced under our unified experimental settings or cited directly from existing studies on weakly supervised WSI classification [36].

## 4.4. Experimental Results

### 4.4.1. Results on the CIFAR-10 Dataset

To evaluate model performance under controllable weak supervision, we conduct extensive experiments on the synthetic CIFAR-10 dataset with varying positive patch ratios (1% to 70%). As summarized in Table 1, DSAGL consistently achieves superior classification performance across all settings. Specifically, at 10%, 20%, 50%, and 70% positive ratios, DSAGL attains instance-level AUCs of 0.9037, 0.9287, 0.9092, and 0.9103, respectively-outperforming strong baselines such as ABMIL, CLAM, and advanced Transformer-based models including TransMIL and IBMIL. At the bag level, DSAGL achieves perfect or near-perfect classification with AUC = 1.0000 in the 20%, 50%, and 70% settings, demonstrating remarkable robustness against label imbalance and noisy instances. Fig. 5 further visualizes the comparative results across positive ratios, validating the consistent performance advantage of DSAGL over existing methods.

To analyze the learning dynamics, we plot the test AUC trajectories over 300 training epochs under the 20% positive patch ratio setting (Fig. 6). All baseline models are reimplemented using publicly available code under identical settings, including the same feature extractor, optimizer, and training schedule, to ensure fair comparison. DSAGL demonstrates fast convergence and stable improvement throughout training, achieving consistently high AUCs at both the instance and bag levels. In contrast, classical methods such as MI-Net, ABMIL, and Gated-ABMIL converge slowly and exhibit noticeable oscillations, while more advanced models like CLAM, TransMIL, and IBMIL display erratic fluctuations or early performance stagnation despite achieving moderate peak AUCs.

These observations highlight the training stability and robustness of DSAGL, attributed to its dual-stream architecture and attention-guided pseudo supervision. The teacher stream, equipped with the FASA module, produces structured multi-scale soft attention maps as reliable supervision signals, while the student stream benefits from fine-grained learning initialized by attention priors. Moreover, the alternating update strategy enables progressive refinement of pseudo labels, mitigating the effect of early noise and enhancing label reliability. This synergy contributes to more stable optimization under weak supervision and improved generalization on noisy instance distributions.

### 4.4.2. Results on the NCT-CRC Dataset

As shown in Table 2, DSAGL consistently outperforms all competing methods across varying positive patch ratios on the NCT-CRC dataset. Its instance-level AUC remains above 0.95 in all cases, reaching as high as 0.9916 at a 70% ratio. This strong performance demonstrates DSAGL’s robustness to morphological variation and distributional shift in real-world histopathological data. At the bag level, DSAGL achieves a perfect AUC of 1.0000 under all settings, matching or exceeding the performance of the best existing MIL approaches.

Fig. 7 provides a visual comparison of instance-level and bag-level AUC trends across different ratios. Unlike competing models, which often exhibit substantial fluctuation or degradation (e.g., CLAM’s instance-level drop at 50%), DSAGL maintains consistent performance as the supervision signal changes. These results confirm the model’s

Table 1

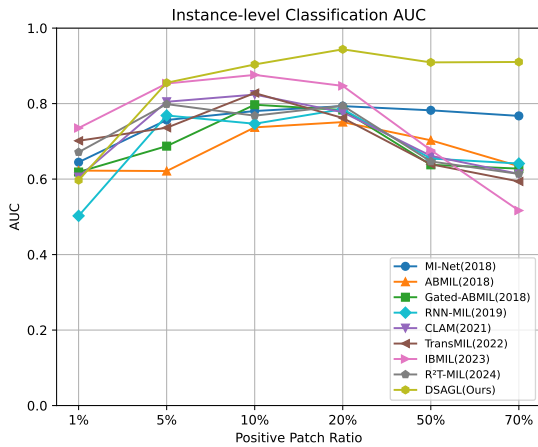
Results on the CIFAR-10 dataset.

(a) Instance-level classification AUC.

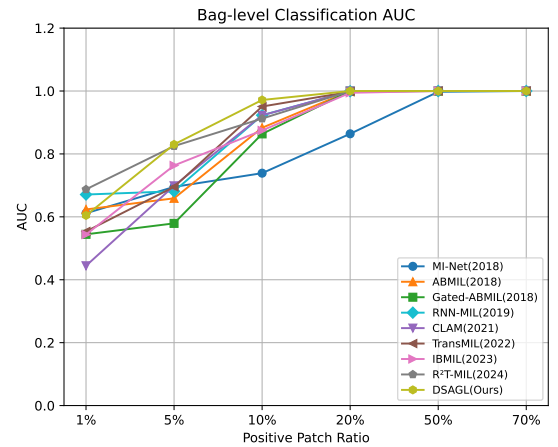
Positive patch ratio	1%	5%	10%	20%	50%	70%
<b>Classical MIL Models</b>						
MI-Net(2018) [48]	0.6447	0.7565	0.7803	0.7933	0.7822	0.7674
RNN-MIL(2019) [4]	0.5026	0.7685	0.7466	0.7852	0.6544	0.6412
<b>Attention-based MIL Models</b>						
ABMIL(2018) [19]	0.6225	0.6213	0.7370	0.7551	0.7028	0.6342
Gated-ABMIL(2018) [19]	0.6187	0.6873	0.7970	0.7831	0.6378	0.6277
CLAM(2021) [31]	0.6054	0.8048	0.8239	0.7771	0.6616	0.6139
<b>Transformer-based or Advanced MIL Models</b>						
TransMIL(2021) [39]	0.7015	0.7360	0.8279	0.7619	0.6393	0.5938
IBMIL(2023) [29]	<b>0.7353</b>	0.8532	0.8760	0.8469	0.6767	0.5167
R <sup>2</sup> T-MIL(2024) [45]	0.6714	0.7986	0.7680	0.7945	0.6468	0.6136
DSAGL(Ours)	0.5971	<b>0.8552</b>	<b>0.9037</b>	<b>0.9287</b>	<b>0.9092</b>	<b>0.9103</b>

(b) Bag-level classification AUC.

Positive patch ratio	1%	5%	10%	20%	50%	70%
<b>Classical MIL Models</b>						
MI-Net(2018) [48]	0.6114	0.6952	0.7388	0.8640	0.9075	<b>1.0000</b>
RNN-MIL(2019) [4]	0.6709	0.6812	0.9230	0.9992	<b>1.0000</b>	<b>1.0000</b>
<b>Attention-based MIL Models</b>						
ABMIL(2018) [19]	0.6235	0.6589	0.8832	<b>1.0000</b>	<b>1.0000</b>	<b>1.0000</b>
Gated-ABMIL(2018) [19]	0.5444	0.5792	0.8637	<b>1.0000</b>	<b>1.0000</b>	<b>1.0000</b>
CLAM(2021) [31]	0.4444	0.6986	0.9226	<b>1.0000</b>	<b>1.0000</b>	<b>1.0000</b>
<b>Transformer-based or Advanced MIL Models</b>						
TransMIL(2022) [39]	0.5536	0.6952	0.9507	0.9976	<b>1.0000</b>	<b>1.0000</b>
IBMIL(2023) [29]	0.5437	0.7633	0.8746	0.9944	<b>1.0000</b>	<b>1.0000</b>
R <sup>2</sup> T-MIL(2024) [45]	<b>0.6874</b>	0.8248	0.9124	<b>1.0000</b>	<b>1.0000</b>	<b>1.0000</b>
DSAGL(Ours)	0.6044	<b>0.8303</b>	<b>0.9715</b>	<b>1.0000</b>	<b>1.0000</b>	<b>1.0000</b>



(a) Instance-level Classification AUC.



(b) Bag-level Classification AUC.

Fig. 5: Comparison of AUC for Different Classification Levels on the CIFAR-10 dataset.

strong generalization capability across heterogeneous tissue patterns and its ability to retain discriminative precision under weak supervision.

#### 4.4.3. Results on the TCGA-Lung dataset

For the real-world TCGA-Lung dataset, Table 3 summarizes the bag-level classification results. Compared to a wide range of representative methods, DSAGL achieves the highest AUC of 0.9727, outperforming CLAM, TransMIL,

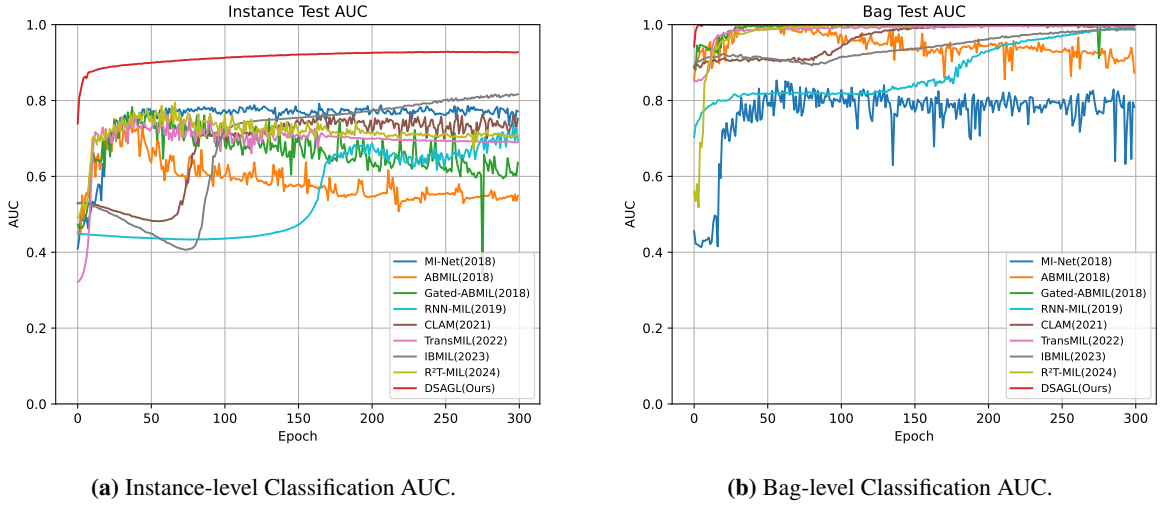


Fig. 6: Test AUC curves on the CIFAR-10 dataset.

Table 2

Results on the NCT-CRC dataset.

(a) Instance-level classification AUC.

Positive patch ratio	10%	20%	50%	70%
<b>Classical MIL Models</b>				
MI-Net(2018) [48]	0.6648	0.6950	0.6996	0.6899
RNN-MIL(2019) [4]	0.6148	0.6234	0.6244	0.6335
<b>Attention-based MIL Models</b>				
ABMIL(2018) [19]	0.6621	0.6424	0.6409	0.6548
Gated-ABMIL(2018) [19]	0.6753	0.6333	0.6830	0.7228
CLAM(2021) [31]	0.6525	0.8525	0.5450	0.6446
<b>Transformer-based or Advanced MIL Models</b>				
TransMIL(2022) [39]	0.7013	0.8530	0.6043	0.6723
IBMIL(2023) [29]	0.7532	0.8542	0.7523	0.8212
R <sup>2</sup> T-MIL(2024) [45]	0.8241	0.8720	0.7656	0.8023
DSAGL(Ours)	<b>0.9731</b>	<b>0.9538</b>	<b>0.9755</b>	<b>0.9916</b>

(b) Bag-level classification AUC.

Positive patch ratio	10%	20%	50%	70%
<b>Classical MIL Models</b>				
MI-Net(2018) [48]	0.7160	0.5185	0.7600	0.7212
RNN-MIL(2019) [4]	0.8201	0.8324	0.9932	<b>1.0000</b>
<b>Attention-based MIL Models</b>				
ABMIL(2018) [19]	0.7407	0.7037	<b>1.0000</b>	<b>1.0000</b>
Gated-ABMIL(2018) [19]	0.9506	0.9506	<b>1.0000</b>	<b>1.0000</b>
CLAM(2021) [31]	0.9828	<b>1.0000</b>	<b>1.0000</b>	<b>1.0000</b>
<b>Transformer-based or Advanced MIL Models</b>				
TransMIL(2022) [39]	0.9723	<b>1.0000</b>	<b>1.0000</b>	<b>1.0000</b>
IBMIL(2023) [29]	<b>1.0000</b>	0.9978	<b>1.0000</b>	<b>1.0000</b>
R <sup>2</sup> T-MIL [45]	<b>1.0000</b>	<b>1.0000</b>	0.9997	<b>1.0000</b>
DSAGL(Ours)	<b>1.0000</b>	<b>1.0000</b>	<b>1.0000</b>	<b>1.0000</b>

and the recent R<sup>2</sup>T-MIL. This strong performance further validates the generalizability and clinical applicability of DSAGL, demonstrating its practical utility in real-world histopathological diagnosis where annotation is limited and data variability is substantial.

## 4.5. Ablation Study

### 4.5.1. Model Architecture Design

To systematically evaluate the contribution of each core component within the DSAGL to classification performance at different granularities, we conducted an ablation study on the NCT-CRC dataset with a positive instance ratio of 10%. The results are summarized in Table 4.

Starting from a baseline model without any additional modules, we observe an instance-level AUC of 0.7410 and a bag-level AUC of 0.9754. Introducing the dual-stream architecture improves the instance-level AUC to 0.8021, while the bag-level AUC reaches 1.0000—indicating that the teacher-student collaborative optimization mechanism effectively enhances bag-level prediction performance. Incorporating the FASA module further boosts the instance-level AUC to 0.9214, demonstrating the effectiveness of multi-scale saliency modeling in identifying diagnostically relevant lesion regions.

Building on this, the addition of the hybrid loss function  $\mathcal{L}_{Hybrid}$  leads to a further increase in instance-level AUC to 0.9348, highlighting the robustness advantages of joint supervision through both hard and soft pseudo labels under weak supervision. Finally, integrating the customized feature encoder VSSMamba into the overall architecture

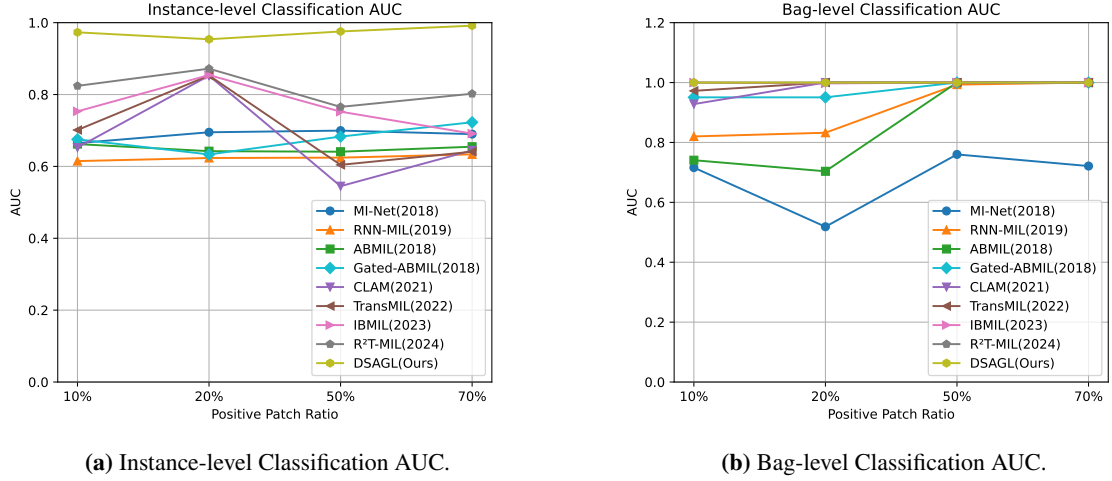


Fig. 7: Comparison of AUC for Different Classification Levels on the NCT-CRC dataset.

Table 3  
Results on the TCGA-Lung dataset.

Method	Bag-level AUC
<i>Classical MIL Models</i>	
MI-Net(2018) [48]	0.9312
RNN-MIL(2019) [4]	0.9307
<i>Attention-based MIL Models</i>	
ABMIL(2018) [19]	0.9488
Gated-ABMIL(2018) [19]	0.9588
CLAM(2021) [31]	0.9607
<i>Transformer-based or Advanced MIL Models</i>	
TransMIL(2021) [39]	0.9672
IBMIL(2023) [29]	0.9689
R <sup>2</sup> T-MIL(2024) [45]	0.9701
DSAGL(Ours)	<b>0.9727</b>

Table 4  
Ablation study on the NCT-CRC dataset.

Dual-stream	FASA	$\mathcal{L}_{Hybrid}$	VSSMamba	Instance AUC	Bag AUC
				0.7410	0.9754
✓				0.8021	<b>1.0000</b>
✓	✓			0.9214	<b>1.0000</b>
✓	✓	✓		0.9348	<b>1.0000</b>
✓	✓	✓	✓	<b>0.9731</b>	<b>1.0000</b>

yields the best performance, achieving an instance-level AUC of 0.9731 while maintaining a bag-level AUC of 1.0000. This result validates the effectiveness of VSSMamba in modeling long-range dependencies and integrating multi-scale features for enhanced instance-level discrimination.

#### 4.5.2. Loss Function Design

To further investigate the contribution of each component in our loss function design, we conduct a series of ablation experiments on the CIFAR-10 dataset with a positive patch ratio of 20%, as summarized in Table 5. These experiments focus on three key factors: whether the binary cross-entropy (BCE) loss is class-balanced, whether knowledge distillation via KL divergence is applied, and what type of pseudo-label is utilized during training.

Under the full configuration (which includes weighted BCE, KL divergence, and soft pseudo-labels), our method achieves the best performance, with an instance-level AUC of 0.9438 and a bag-level AUC of 1.0000. Removing the

**Table 5**

Ablation study on the effects of pseudo-label design, KL divergence, and weighted BCE on the CIFAR-10 dataset.

Weighted BCE	KL Divergence	Pseudo-label Type	Instance AUC	Bag AUC
✓	✓	Soft	<b>0.9438</b>	<b>1.0000</b>
✓		Soft	0.9317	<b>1.0000</b>
		Soft	0.9031	0.9814
✓	✓	Hard	0.9123	<b>1.0000</b>
✓		Random	0.6124	0.6749
✓		GT	0.9420	<b>1.0000</b>

KL divergence term leads to a noticeable drop in instance AUC to 0.9317, indicating that mimicking the teacher’s soft outputs significantly enhances the student’s representational learning.

Further eliminating the class-balancing mechanism in BCE results in a more pronounced performance degradation: the instance AUC decreases to 0.9031 and the bag-level AUC falls to 0.9814. This suggests that class imbalance adversely affects optimization, and that the reweighted BCE term contributes to better training stability.

When the soft pseudo-labels are binarized into hard labels, the instance AUC declines to 0.9123, even though KL divergence is retained. This underscores the importance of preserving uncertainty information in the pseudo-labels to guide the student more effectively. Moreover, when pseudo-labels are randomly assigned, performance drops drastically, with the instance AUC and bag-level AUC plunging to 0.6124 and 0.6749, respectively highlighting the critical role of pseudo-label quality in weakly supervised learning.

As a reference upper bound, we also evaluate a student model trained with ground-truth instance labels, which yields an instance-level AUC of 0.9420 and a bag-level AUC of 1.0000. While slightly lower than the full hybrid loss configuration, this result demonstrates that our pseudo-labeling strategy is already approaching the performance of fully supervised training.

Overall, these findings confirm that the proposed hybrid loss, which integrates confidence-aware supervision, class-balanced reweighting, and soft-label distillation, is critical for achieving robust and generalizable learning under weak supervision.

#### 4.6. Visualization and Analysis

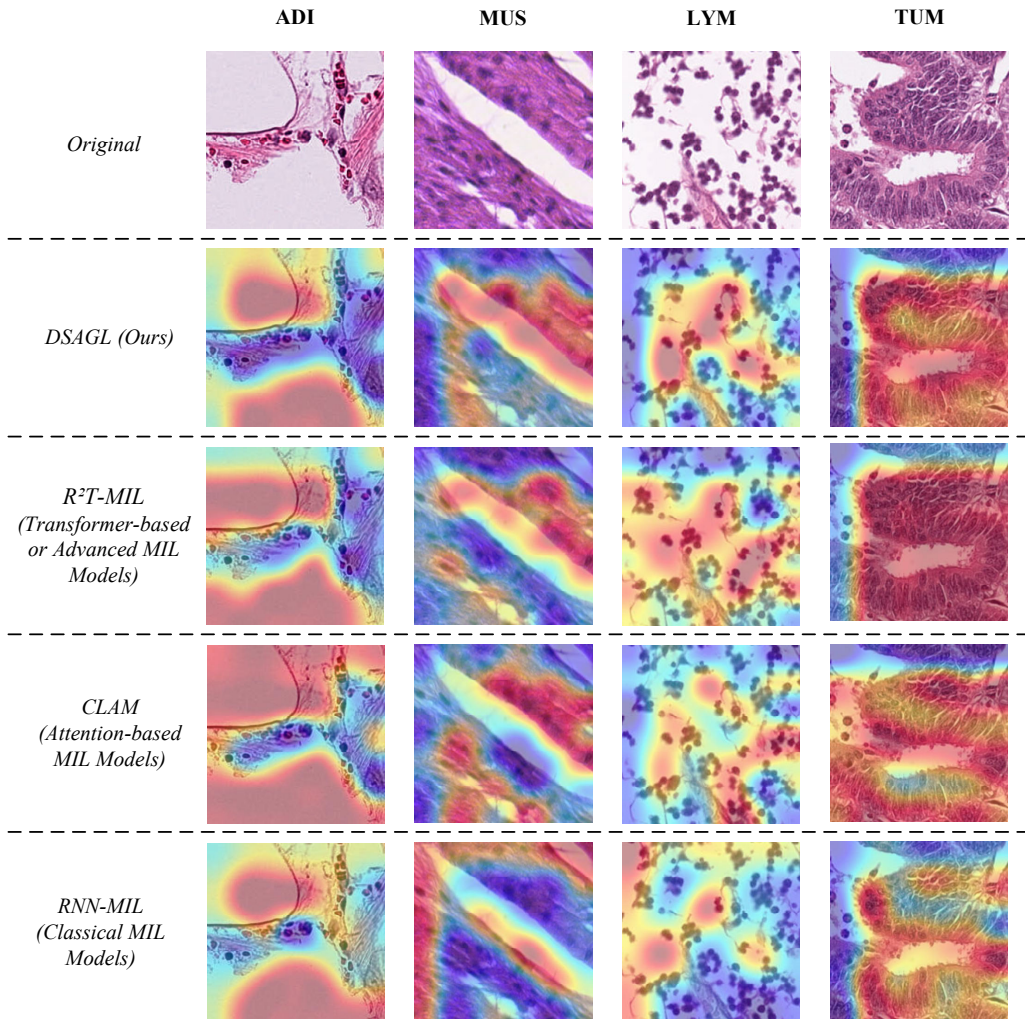
To further interpret the spatial reasoning behavior of DSAGL and compare its attention mechanisms with representative MIL models, we visualize class-discriminative attention responses from the student branch. Specifically, Grad-CAM is applied to the final convolutional layer of the student encoder, where gradients are backpropagated from the classification logits to generate saliency heatmaps. These visualizations highlight the regions the model attends to during inference and provide insight into its learned instance-level representations.

Fig. 8 presents a qualitative comparison of attention heatmaps across four representative tissue classes—ADI, MUS, LYM, and TUM from the NCT-CRC dataset. The top row displays the original histopathology images, followed by visualizations from four MIL models representing distinct architectural paradigms: DSAGL (ours, representing Transformer-based or advanced MIL), R<sup>2</sup>T-MIL (recent Transformer-based MIL), CLAM (attention-based MIL), and RNN-MIL (classical MIL with pooling). This selection enables a cross-generational comparison of spatial reasoning capabilities among MIL designs.

Across all tissue types, DSAGL generates attention maps that are consistently more focused, compact, and semantically aligned with diagnostic regions. In the ADI class (adipose tissue), DSAGL effectively suppresses homogeneous background and highlights interstitial boundaries, whereas other methods yield dispersed or poorly localized activation. For MUS (muscle), DSAGL sharply delineates fiber margins, while R<sup>2</sup>T-MIL and CLAM produce broader, less discriminative responses. In the LYM class (lymphocyte), which is challenging due to its sparse distribution, DSAGL accurately localizes small lymphocyte clusters, outperforming CLAM’s overextended focus and RNN-MIL’s weak saliency. For TUM (tumor), DSAGL concentrates on epithelial abnormalities and distorted glandular structures with superior boundary precision.

Despite these strengths, some failure cases are observed. In certain MUS samples, attention maps slightly extend into adjacent connective tissue, potentially due to noisy pseudo labels in the early training stages. A similar phenomenon appears in LYM patches, suggesting pseudo-supervision inconsistencies in sparsely distributed lesions.

Overall, the alternating teacher-student optimization and hybrid supervision strategy in DSAGL effectively reduce attention drift. Through iterative pseudo-label refinement and instance-level consistency enforcement, the model achieves more stable and diagnostically meaningful attention localization. These interpretable saliency patterns further demonstrate DSAGL’s applicability and reliability in real-world weakly supervised histopathology tasks.



**Fig. 8:** Qualitative comparison of attention heatmaps on four tissue classes (ADI, MUS, LYM, TUM) from the NCT-CRC dataset. Each row corresponds to a representative MIL model: DSAGL (Ours), R<sup>2</sup>T-MIL (Transformer-based), CLAM (Attention-based), and RNN-MIL (Classical pooling-based). DSAGL produces more localized and diagnosis-relevant attention responses across all tissue types.

## 5. Discussion

The proposed DSAGL framework demonstrates several strengths in the context of weakly supervised WSI classification. By introducing a dual-branch architecture, the model effectively bridges the supervision gap between bag-level labels and instance-level learning. The alternating training strategy facilitates bidirectional knowledge transfer between the teacher and student branches, enhancing semantic consistency and training stability. Furthermore, the integration of a mamba-based encoder enables efficient modeling of long-range dependencies across image patches while maintaining linear computational complexity. Experimental results across multiple datasets confirm that DSAGL

outperforms state-of-the-art MIL methods, particularly in terms of instance-level precision and boundary localization accuracy.

Nevertheless, some limitations remain. First, in scenarios with highly imbalanced patch distributions or extremely sparse positive regions, the pseudo labels generated by the teacher branch may be noisy during the early stages of training, potentially affecting the convergence of the student branch. Second, the current Mamba encoder treats patch sequences as one-dimensional inputs, which may fail to capture essential two-dimensional spatial structures and anatomical priors inherent in histopathological images. Third, DSAGL does not explicitly model pseudo-label uncertainty, which could reduce robustness in regions with ambiguous or noisy annotations.

Overall, DSAGL is well suited for high-resolution, structurally complex, and weakly annotated pathological images, demonstrating strong generalization across diverse data distributions. Future work will focus on enhancing the dual-branch learning paradigm by designing more adaptive feature extractors and incorporating uncertainty-aware training objectives to improve robustness and interpretability in complex pathological contexts. In addition, extending DSAGL to multi-modal inputs or integrating it with pre-trained vision models holds promise for improving its practicality and generalizability.

## 6. Conclusion

In this work, we propose DSAGL, a novel dual-branch teacher-student framework for weakly supervised WSI classification. By integrating attention-guided pseudo-labeling and an alternating training strategy, DSAGL effectively bridges the gap between coarse-grained supervision and fine-grained instance-level learning. The incorporation of a Mamba-based encoder enables efficient modeling of long-range dependencies with linear complexity, allowing the model to process large-scale instance sets while preserving global context. Additionally, the FASA module enhances the model's ability to focus on sparse yet diagnostically significant regions through multi-scale attention. Experimental results on three benchmark datasets demonstrate that DSAGL consistently outperforms existing MIL-based approaches in both instance-level and bag-level classification tasks, particularly under challenging conditions such as low positive-instance ratios and heterogeneous lesion patterns. These findings highlight the effectiveness, scalability, and generalization potential of DSAGL, making it a promising solution for real-world computational pathology applications.

## CRedit authorship contribution statement

**Daoxi Cao:** Conceptualization of this study, Methodology, Software, Validation, Formal analysis, Writing - Original Draft, Visualization. **Hangbei Cheng:** Conceptualization of this study, Methodology, Writing - Review & Editing. **Yijin Li:** Conceptualization of this study, Writing - Review & Editing. **Ruolin Zhou:** Conceptualization of this study, Validation, Investigation. **Xuehan Zhang:** Conceptualization of this study, Validation, Formal analysis. **Xinyi Li:** Conceptualization of this study, Validation, Formal analysis. **Binwei Li:** Conceptualization of this study, Validation, Investigation. **Xuancheng Gu:** Conceptualization of this study, Data Curation, Visualization. **Xueyu Liu:** Conceptualization of this study, Project administration, Supervision. **Yongfei Wu:** Conceptualization of this study, Project administration, Methodology, Supervision.

## Declaration of competing interest

The authors declare that they have no known competing financial interests or personal relationships that could have appeared to influence the work reported in this paper.

## Acknowledgments

This research did not receive any specific grant from funding agencies in the public, commercial, or not-for-profit sectors.

## Data availability

Data will be made available on request.

## References

- [1] Alex, K., Sutskever, I., Hinton, G.E., 2011. Imagenet classification with deep convolutional networks, in: volume-1; pages-1097–1105; NIPS'12 Proceedings of the 25th International Conference on Neural Information Processing System.
- [2] Alzubaidi, L., Zhang, J., Humaidi, A.J., Al-Dujaili, A., Duan, Y., Al-Shamma, O., Santamaría, J., Fadhel, M.A., Al-Amidie, M., Farhan, L., 2021. Review of deep learning: concepts, cnn architectures, challenges, applications, future directions. *Journal of big Data* 8, 1–74.
- [3] Amores, J., 2013. Multiple instance classification: Review, taxonomy and comparative study. *Artificial intelligence* 201, 81–105.
- [4] Campanella, G., Hanna, M.G., Geneslaw, L., Mirafior, A., Werneck Krauss Silva, V., Busam, K.J., Brogi, E., Reuter, V.E., Klimstra, D.S., Fuchs, T.J., 2019. Clinical-grade computational pathology using weakly supervised deep learning on whole slide images. *Nature medicine* 25, 1301–1309.
- [5] Chen, Y., Li, M., Wu, Y., Liu, X., Hao, F., Zhou, D., Zhou, X., Wang, C., 2020. Msa-mil: A deep residual multiple instance learning model based on multi-scale annotation for classification and visualization of glomerular spikes. *arXiv preprint arXiv:2007.00858*.
- [6] Cheng, H., Liu, X., Zhang, J., Dong, X., Ma, X., Zhang, Y., Meng, H., Chen, X., Yue, G., Li, Y., et al., 2025. Glmkd: Joint global and local mutual knowledge distillation for weakly supervised lesion segmentation in histopathology images. *Expert Systems with Applications* 279, 127425.
- [7] Chua, L.O., Roska, T., 1993. The cnn paradigm. *IEEE Transactions on Circuits and Systems I: Fundamental Theory and Applications* 40, 147–156.
- [8] Dimitriou, N., Arandjelović, O., Caie, P.D., 2019. Deep learning for whole slide image analysis: an overview. *Frontiers in medicine* 6, 264.
- [9] Dosovitskiy, A., Beyer, L., Kolesnikov, A., Weissenborn, D., Zhai, X., Unterthiner, T., Dehghani, M., Minderer, M., Heigold, G., Gelly, S., et al., 2020. An image is worth 16x16 words: Transformers for image recognition at scale. *arXiv preprint arXiv:2010.11929*.
- [10] Du, F., Yang, P., Jia, Q., Nan, F., Chen, X., Yang, Y., 2023. Global and local mixture consistency cumulative learning for long-tailed visual recognitions, in: *Proceedings of the IEEE/CVF conference on computer vision and pattern recognition*, pp. 15814–15823.
- [11] Farahani, N., Parwani, A.V., Pantanowitz, L., 2015. Whole slide imaging in pathology: advantages, limitations, and emerging perspectives. *Pathology and Laboratory Medicine International*, 23–33.
- [12] Gu, A., Dao, T., 2023. Mamba: Linear-time sequence modeling with selective state spaces. *arXiv preprint arXiv:2312.00752*.
- [13] Gu, A., Goel, K., Ré, C., 2021. Efficiently modeling long sequences with structured state spaces. *arXiv preprint arXiv:2111.00396*.
- [14] Han, K., Wang, Y., Chen, H., Chen, X., Guo, J., Liu, Z., Tang, Y., Xiao, A., Xu, C., Xu, Y., et al., 2022. A survey on vision transformer. *IEEE transactions on pattern analysis and machine intelligence* 45, 87–110.
- [15] Han, K., Xiao, A., Wu, E., Guo, J., Xu, C., Wang, Y., 2021. Transformer in transformer. *Advances in neural information processing systems* 34, 15908–15919.
- [16] Hanley, J.A., McNeil, B.J., 1982. The meaning and use of the area under a receiver operating characteristic (roc) curve. *Radiology* 143, 29–36.
- [17] Hao, J., He, L., Hung, K.F., 2024. T-mamba: Frequency-enhanced gated long-range dependency for tooth 3d cbct segmentation. *arXiv e-prints*, arXiv:2404.
- [18] Hou, W., Yu, L., Lin, C., Huang, H., Yu, R., Qin, J., Wang, L., 2022. H<sup>2</sup>-mil: exploring hierarchical representation with heterogeneous multiple instance learning for whole slide image analysis, in: *Proceedings of the AAAI conference on artificial intelligence*, pp. 933–941.
- [19] Ilse, M., Tomczak, J., Welling, M., 2018. Attention-based deep multiple instance learning, in: *International conference on machine learning*, PMLR. pp. 2127–2136.
- [20] Jiang, Q., Xiao, Y., Hong, A.N., Gao, Z., Shen, Y., Fan, Q., Feng, P., Zhong, W., 2022. Bimetallic metal–organic framework fe/co-mil-88 (nh<sub>2</sub>) exhibiting high peroxidase-like activity and its application in detection of extracellular vesicles. *ACS Applied Materials & Interfaces* 14, 41800–41808.
- [21] Kather, J.N., Weis, C.A., Bianconi, F., Melchers, S.M., Schad, L.R., Gaiser, T., Marx, A., Zöllner, F.G., 2016. Multi-class texture analysis in colorectal cancer histology. *Scientific reports* 6, 1–11.
- [22] Kingma, D.P., Ba, J., 2014. Adam: A method for stochastic optimization. *arXiv preprint arXiv:1412.6980*.
- [23] Krizhevsky, A., Hinton, G., et al., 2009. Learning multiple layers of features from tiny images.
- [24] Kullback, S., Leibler, R.A., 1951. On information and sufficiency. *The annals of mathematical statistics* 22, 79–86.
- [25] LeCun, Y., Boser, B., Denker, J.S., Henderson, D., Howard, R.E., Hubbard, W., Jackel, L.D., 1989. Backpropagation applied to handwritten zip code recognition. *Neural computation* 1, 541–551.
- [26] Li, B., Li, Y., Eliceiri, K.W., 2021. Dual-stream multiple instance learning network for whole slide image classification with self-supervised contrastive learning, in: *Proceedings of the IEEE/CVF conference on computer vision and pattern recognition*, pp. 14318–14328.
- [27] Li, H., Zhu, C., Zhang, Y., Sun, Y., Shui, Z., Kuang, W., Zheng, S., Yang, L., 2023a. Task-specific fine-tuning via variational information bottleneck for weakly-supervised pathology whole slide image classification, in: *Proceedings of the IEEE/CVF conference on computer vision and pattern recognition*, pp. 7454–7463.
- [28] Li, K., Qian, Z., Han, Y., Chang, E.I.C., Wei, B., Lai, M., Liao, J., Fan, Y., Xu, Y., 2023b. Weakly supervised histopathology image segmentation with self-attention. *Medical Image Analysis* 86, 102791.
- [29] Lin, T., Yu, Z., Hu, H., Xu, Y., Chen, C.W., 2023. Interventional bag multi-instance learning on whole-slide pathological images, in: *Proceedings of the IEEE/CVF Conference on Computer Vision and Pattern Recognition*, pp. 19830–19839.
- [30] Liu, Z., Ning, J., Cao, Y., Wei, Y., Zhang, Z., Lin, S., Hu, H., 2022. Video swin transformer, in: *Proceedings of the IEEE/CVF conference on computer vision and pattern recognition*, pp. 3202–3211.
- [31] Lu, M.Y., Williamson, D.F., Chen, T.Y., Chen, R.J., Barbieri, M., Mahmood, F., 2021. Data-efficient and weakly supervised computational pathology on whole-slide images. *Nature Biomedical Engineering* 5, 555–570.
- [32] Ma, J., Li, F., Wang, B., 2024. U-mamba: Enhancing long-range dependency for biomedical image segmentation. *arXiv preprint arXiv:2401.04722*.
- [33] Mao, A., Mohri, M., Zhong, Y., 2023. Cross-entropy loss functions: Theoretical analysis and applications, in: *International conference on Machine learning*, PMLR. pp. 23803–23828.

- [34] Nakhli, R., Moghadam, P.A., Mi, H., Farahani, H., Baras, A., Gilks, B., Bashashati, A., 2023. Sparse multi-modal graph transformer with shared-context processing for representation learning of giga-pixel images, in: Proceedings of the IEEE/CVF Conference on Computer Vision and Pattern Recognition, pp. 11547–11557.
- [35] Niazi, M.K.K., Parwani, A.V., Gurcan, M.N., 2019. Digital pathology and artificial intelligence. *The lancet oncology* 20, e253–e261.
- [36] Qu, L., Wang, M., Song, Z., et al., 2022. Bi-directional weakly supervised knowledge distillation for whole slide image classification. *Advances in Neural Information Processing Systems* 35, 15368–15381.
- [37] Robbins, H., Monro, S., 1951. A stochastic approximation method. *The annals of mathematical statistics* , 400–407.
- [38] Ryu, J., Puche, A.V., Shin, J., Park, S., Brattoli, B., Lee, J., Jung, W., Cho, S.I., Paeng, K., Ock, C.Y., et al., 2023. Ocelot: overlapped cell on tissue dataset for histopathology, in: Proceedings of the IEEE/CVF Conference on Computer Vision and Pattern Recognition, pp. 23902–23912.
- [39] Shao, Z., Bian, H., Chen, Y., Wang, Y., Zhang, J., Ji, X., et al., 2021. Transmil: Transformer based correlated multiple instance learning for whole slide image classification. *Advances in neural information processing systems* 34, 2136–2147.
- [40] Shi, J., Li, C., Gong, T., Zheng, Y., Fu, H., 2024. Vila-mil: Dual-scale vision-language multiple instance learning for whole slide image classification, in: Proceedings of the IEEE/CVF Conference on Computer Vision and Pattern Recognition, pp. 11248–11258.
- [41] Shi, J., Tang, L., Li, Y., Zhang, X., Gao, Z., Zheng, Y., Wang, C., Gong, T., Li, C., 2023. A structure-aware hierarchical graph-based multiple instance learning framework for pt staging in histopathological image. *IEEE Transactions on Medical Imaging* 42, 3000–3011.
- [42] Shmatko, A., Ghaffari Laleh, N., Gerstung, M., Kather, J.N., 2022. Artificial intelligence in histopathology: enhancing cancer research and clinical oncology. *Nature cancer* 3, 1026–1038.
- [43] Song, A.H., Jaume, G., Williamson, D.F., Lu, M.Y., Vaidya, A., Miller, T.R., Mahmood, F., 2023. Artificial intelligence for digital and computational pathology. *Nature Reviews Bioengineering* 1, 930–949.
- [44] Tang, W., Huang, S., Zhang, X., Zhou, F., Zhang, Y., Liu, B., 2023. Multiple instance learning framework with masked hard instance mining for whole slide image classification, in: Proceedings of the IEEE/CVF International Conference on Computer Vision, pp. 4078–4087.
- [45] Tang, W., Zhou, F., Huang, S., Zhu, X., Zhang, Y., Liu, B., 2024. Feature re-embedding: Towards foundation model-level performance in computational pathology, in: Proceedings of the IEEE/CVF Conference on Computer Vision and Pattern Recognition, pp. 11343–11352.
- [46] Vaswani, A., Shazeer, N., Parmar, N., Uszkoreit, J., Jones, L., Gomez, A.N., Kaiser, Ł., Polosukhin, I., 2017. Attention is all you need. *Advances in neural information processing systems* 30.
- [47] Wan, F., Liu, C., Ke, W., Ji, X., Jiao, J., Ye, Q., 2019. C-mil: Continuation multiple instance learning for weakly supervised object detection, in: Proceedings of the IEEE/CVF conference on computer vision and pattern recognition, pp. 2199–2208.
- [48] Wang, X., Yan, Y., Tang, P., Bai, X., Liu, W., 2018. Revisiting multiple instance neural networks. *Pattern recognition* 74, 15–24.
- [49] Wu, K., Jiang, Z., Tang, K., Shi, J., Xie, F., Wang, W., Wu, H., Zheng, Y., 2024. Pan-cancer histopathology wsi pre-training with position-aware masked autoencoder. *IEEE Transactions on Medical Imaging* .
- [50] Zhang, H., Meng, Y., Zhao, Y., Qiao, Y., Yang, X., Coupland, S.E., Zheng, Y., 2022a. Dtf-d-mil: Double-tier feature distillation multiple instance learning for histopathology whole slide image classification, in: Proceedings of the IEEE/CVF conference on computer vision and pattern recognition, pp. 18802–18812.
- [51] Zhang, L., Chen, X., Dong, R., Ma, K., 2022b. Region-aware knowledge distillation for efficient image-to-image translation. *arXiv preprint arXiv:2205.12451* .
- [52] Zhu, L., Liao, B., Zhang, Q., Wang, X., Liu, W., Wang, X., . Vision mamba: Efficient visual representation learning with bidirectional state space model, in: Forty-first International Conference on Machine Learning.